A comparison of the SeaWiFS chlorophyll and CZCS pigment algorithms using optical data from the 1992 JGOFS Equatorial Pacific Time Series

W. JOSEPH RHEA* and CURTISS O. DAVIS*

Abstract—Optical data were collected during two U.S. JGOFS EqPac Time Series cruises aboard the U.S. Research Vessel Thomas G. Thompson, at a station at 140°W on the equator, during the time of both the first equinox and the second equinox of 1992. This data set represents the range of conditions expected in this region, and was used to compare the SeaWiFS chlorophyll *a* algorithm with the CZCS pigment algorithm, as well as test the validity of using ocean color remote sensing to track the biological response to physical phenomena such as Kelvin Waves and Tropical Instability Waves (TIW). Time Series I (23 March to 9 April) took place during the maximum expression of the 1991–92 El Niño event, and coincided with the peak of a passing Kelvin wave. Time Series II (2–21 October) occurred during La Niña conditions and encompassed the passage of a TIW. The SeaWiFS pigment compared favorably with the earlier CZCS pigment algorithm and indicate that the SeaWiFS algorithm is capable of determining both quantitative and qualitative changes in surface chlorophyll *a* from remotely sensed optical data in high nutrient, low chlorophyll regions such as the Equatorial Pacific. Our results show that, although Kelvin waves can not be currently tracked using ocean color sensors alone, when a Kelvin wave is detected by other methods, satellite ocean color data can be used to characterize the biological response to the Kelvin wave. However, since TIWs have a much shorter period and can enhance near-surface phytoplankton growth rates quickly, they can be tracked using remotely sensed ocean color data using either the CZCS pigment or the SeaWiFS chlorophyll algorithm. © 1998 Elsevier Science Ltd. All rights reserved

INTRODUCTION

One of the primary goals of the Joint Global Ocean Flux Study's (JGOFS) Equatorial Pacific (EqPac) experiment in 1992 was to assess the causes of the high nutrient, low chlorophyll (HNLC) phenomenon, including iron limitation and grazing pressure, and to evaluate the role of the equatorial upwelling system in the global carbon cycle (Murray *et al.*, 1995). While detailed studies were possible during the field year, long term monitoring requires alternative techniques, such as measurements from moorings and satellite remote sensing.

Our participation in EqPac was to collect optical data to establish a link between the biological and chemical processes measured by the other participants and the optical properties that could be sensed by satellite ocean color remote sensing. A specific goal was to assess the validity of a new algorithm for chlorophyll *a* and Colored Dissolved Organic Matter (CDOM) (Carder *et al.*, Submitted) that is planned to be used for the Sea viewing Wide Field-of-view Sensor (SeaWiFS; Hooker *et al.*, 1992) onboard the SeaStar satellite that was launch on August 1, 1997. For this paper, the SeaWiFS algorithm was compared to

---

* Code 7212, Naval Research Laboratory, Washington, DC, 20375 USA.

an existing pigment algorithm developed for the Coastal Zone Color Scanner (CZCS) using both above-water and below-water optical data collected during two Time Series cruises aboard the U.S. Research Vessel Thomas G. Thompson in 1992.

The equatorial Pacific Ocean is noted for its role in the interannual cycle known as El Niño /Southern Oscillation (ENSO), which has a strong impact on global atmospheric circulation (Philander, 1990). Two important dynamic phenomena in this region are eastward-propagating Kelvin waves and westward-propagating Tropical Instability Waves (TIW). Kelvin waves are characterized by 40–70 day periods, zonal wavelengths of up to 10,000 km, and phase speeds of 200 km/day in the first baroclinic mode, and are associated with typical El Niño conditions (Knox and Halpern, 1982; Eriksen *et al.*, 1983; Johnson and McPhaden, 1993). Tropical Instability Waves are characterized by 20–30 day periods, Zonal wavelengths of 500–1500 km, and phase speeds of approximately 50 km /day (e.g., see Legeckis, 1977; Halpern *et al.*, 1988).

TIWs in this region are caused by the large latitudinal shear of the surface currents, especially that of the westward jet just north of the equator (Philander, 1990), and tend to be suppressed during El Niño conditions (Philander *et al.*, 1985; Kessler and McPhaden, 1995) as well as seasonally during April and May, when winds and surface currents are reduced. These physical phenomena have a profound effect on the chemistry and biology of the equatorial Pacific. Kelvin waves bring warm, low-nutrient water from the eastern equatorial Pacific into the western Pacific. This, coupled with the lower wind stress and reduced equatorial upwelling associated with El Niño, results in a reduction of the phytoplankton biomass and productivity in the eastern equatorial Pacific during El Niño. TIWs transport water to the north of the equator during non-El Niño, or La Niña, conditions and therefore enhance the normal equatorial upwelling, drawing more high chlorophyll and high-nutrient water to the surface near the equator. Although upwelling brings large amounts of nutrients to the surface, in the equatorial Pacific, phytoplankton productivity is only moderately enhanced and hence chlorophyll concentrations remain fairly low (Chisholm and Morel, 1991; Cullen, 1995).

Under these prevailing high-light and high-nutrient conditions, phytoplankton may change the ratio of accessory pigments to chlorophyll a, and possibly add protective pigments (Lindley *et al.*, 1995). Either of these conditions could affect the accuracy of the SeaWiFS algorithm, which was originally developed using data primarily from subtropical regions. If the SeaWiFS algorithm works well for the equatorial region under these conditions, then SeaWiFS and other new sensors planned for launch in the next few years such as the National Aeronautics and Space Administration's Moderate Resolution Imaging Spectroradiometer (MODIS), and European Space Agency's Medium Resolution Imaging Spectrometer (MERIS) may be used to monitor the biological dynamics of the equatorial Pacific.

METHODS

Study area

Optical data were collected during two U. S. JGOFS EqPac Time Series cruises aboard the U.S. Research Vessel Thomas G. Thompson, at a station at 140°W on the equator. Time Series I (Thompson cruise number TT008) ran from 23 March to 9 April, 1992 (Local Year Day 83–100). Time Series II (Thompson cruise number TT012) ran from 2-21 October (Local Year Day 276–295).

Sample collection

In-water optical profile data were collected following SeaWiFS protocols (Mueller and Austin, 1995), using a Bio-Optical Profiling System (BOPS), which is an updated version of the system originally developed by Smith *et al.* (1984). The package contains a Biospherical Instruments MER-1048 Spectroradiometer (MER), a Sea-Bird CTD, a Sea Tech fluorometer, and a Sea Tech 25-cm transmissometer. The data collected by the MER include downwelling spectral irradiance $E_d(z,\lambda)$, upwelling spectral irradiance $E_u(z,\lambda)$, upwelling spectral radiance $L_u(z,\lambda)$, Photosynthetically Available Radiation PAR(z), surface spectral irradiance $E_s(\lambda)$, temperature, conductivity, chlorophyll *a* fluorescence, and beam attenuation. In-water optical profile data to 200 m were collected once per day, at the same time each day, for the duration of each time series. Profiles were taken off the stern of the ship using the BOPS attached to a crane which extended 7 m beyond the stern. The ship is sharply undercut on the stern so that the instrument package was more than 10 m away from the ship at the waterline. In addition, the ship was positioned so that the sun was aft of the ship during the measurement to reduce ship shadow.

At the same time, above-water sea surface reflectance spectra (512 contiguous bands at 1.426 nm sampling frequency, ranging from approximately 350 nm to 1000 nm) were measured using a hand-held Analytical Spectral Devices (ASD; Boulder, CO) Personal Spectrometer-II (PS-II). The procedure for measuring reflectance was a modified version of Carder and Steward (1985). Five sets of measurements of a gray 10% reflectance Spectralon plaque (Labsphere, Inc., North Sutton, NH), the sea surface and the section of the sky that would be reflected off the sea surface at the measurement angle are made in rapid succession. A polarizer was not used and measurements were made at 90° azimuthal angle to the sun and at a 30° angle relative to the vertical to minimize reflected sunlight.

Chlorophyll data

The chlorophyll *a* data used in this study were collected at discrete depths from morning hydrocasts approximately four hours before the in-water profiles and above-water reflectance measurements were taken. Although chlorophyll *a* data were collected daily during the 20-day Time Series I, only 16 points were used here as they contained both 0 m and 15 m samples. Similarly, during the 19-day Time Series II, 16 chlorophyll *a* data points were used because they contained both 0 m and 15 m samples. Dr. Robert R. Bidigare of the University of Hawaii at Manoa processed the data as part the JGOFS EqPac core measurement program. Chlorophyll *a* and phaeopigments were measured by high performance liquid chromatography (HPLC) pigment analysis (Bidigare and Ondrusek, Submitted). The chlorophyll *a* data were retrieved electronically from the JGOFS Home Page (URL Address; http://www1.whoi.edu/jgofs.html) on 28 December, 1995. The chlorophyll *a* data retrieved were listed as Version April 10, 1994, and remain the current version as of the submission date of this paper. Phaeopigments were virtually non-existent in either of the time series data sets (R. R. Bidigare, personal communication). Therefore, the data are valid for comparing with both the SeaWiFS algorithm that separates detrital components from chlorophyll *a*, and with the CZCS algorithm, which is based on a regression against chlorophyll plus phaeopigments.

As a means of ground-truthing pigment algorithms, two methods have been employed to determine the surface chlorophyll *a* that could be measured accurately by a satellite. In the

Carder *et al.* (Submitted) paper, the SeaWiFS algorithm was compared to measured chlorophyll *a* at 0m depth (usually recorded from a bucket cast or a near-surface bottle cast). A second common method is to calculate C_{sat} (chlorophyll concentrations detectable by a satellite), which is calculated by taking a mean of the measured chlorophyll *a* data within the first light attenuation depth (Smith and Baker, 1978). In this study, chlorophyll *a* concentrations were measured at 0 m and 15 m depth intervals on both time series, and since the first light attenuation depth was approximately 17 m for both time series, the surface and 15 meter chlorophyll *a* records were simply averaged to approximate C_{sat}. A comparison of measured surface chlorophyll *a* and derived C_{sat} (see Fig. 1) shows little difference during either time series, which is expected since the upper 20 m of the water column was well mixed during both time series. Therefore, measured surface chlorophyll *a* is used as ground truth for this paper.

Processing of optical data

The in-water data were processed in two levels, as described in Siegel *et al.* (1995). The first level cleaned the raw profile data and binned them into 1-meter intervals. Either the downcast or upcast was used, depending on freedom from clouds, absence of data spikes and data dropouts. The next step was an automated process to remove any remaining data spikes or dropouts and replace them (typically single values) with interpolated values. The data were then checked for single points lying outside of 2 standard deviations of a 7-point running mean, and any outlying points were then replaced with interpolated values. This was done to remove effects caused by wave-focusing in clear waters. The "cleaned" data were then mean-binned into 1-meter intervals, centered on the half meter.

The second level of processing involved interactive spectral processing of the optical portion of the data file. First, ship-roll was removed from surface light channels when necessary, by applying a 7-point running mean filter to each of the 4 surface light channels. Next, cloud shadows were removed from the underwater light field by normalizing each underwater optical channel to the maximum of the closest matching surface light wavelength. Also, when needed, the surface light channel records were "shifted" slightly in time before normalizing to account for difference between the time a cloud passed over the surface array and underwater array. This shifting was used only for normalizing and was not applied to the final surface light data. Next, sea surface wave effects were removed from underwater optical channels by applying either a 3-point, 5-point, or 7-point running mean filter to all underwater optical channels. This smoothing process was repeated from 1 to 99 times to remove fully all remaining optical aberrations.

The above-water data from the PS-II were processed using a combination of software developed by Analytical Spectral Devices and by the authors. Multiple samples were averaged together and the results were used to calculate the optical properties described below.

Calculation of optical properties

Water-leaving radiance, $L_w(\lambda)$, was calculated from the in-water data using the formula

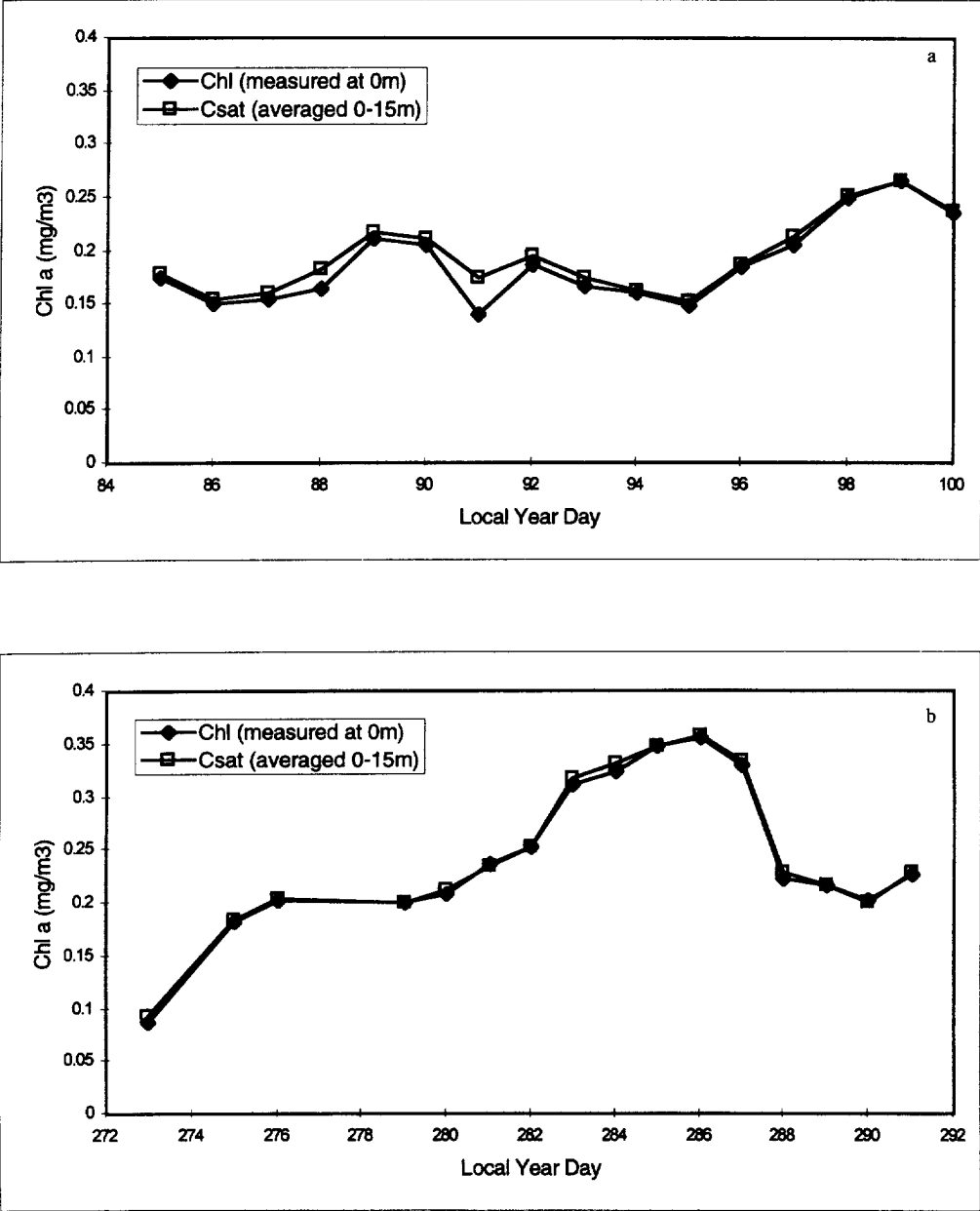$$L_w(\lambda) = (t/n^2)L_u(0^-, \lambda), \tag{1}$$

Fig. 1. a. Comparison of surface Chlorophyll concentration and C_{sat} derived from averaging surface and 15m concentrations for Time Series I. b. Comparison of surface Chlorophyll concentration and C_{sat} derived from averaging surface and 15m concentrations for Time Series II.

where $L_u(0^-,\lambda)$ (upwelling spectral radiance just below the sea-sky interface) is calculated by performing a least squares fit of the upper 5 m of $L_u(z,\lambda)$ (upwelling spectral radiance) profile and projecting a line to a depth of 0.0 m, and t/n^2 accounts for the loss at the sea surface from transmittance across the surface from the index of refraction n from water to air. For a near zenith Sun, a nadir viewing instrument, and a calm surface, $t \approx 0.98$ and $n \gg (1.341$, therefore $t/n^2 \approx 0.544$ (Austin, 1974).

Remote sensing reflectance, $R_{rs}(\lambda)$, the ratio of water leaving radiance to downwelling surface irradiance just above the sea surface, was calculated from in-water data using the formula

$$R_{rs}(\lambda) = L_w(\lambda)/E_d(0^+, \lambda), \qquad (2)$$

where $E_d(0^+,\lambda)$ (spectral irradiance just above the sea-sky interface) was calculated using the equation

$$E_d(0^+, \lambda) = E_d(0^-, \lambda)/0.96, \qquad (3)$$

$E_d(0^-,\lambda)$ (downwelling spectral radiance just below the sea-sky interface) was calculated by performing a least squares fit of the upper 5 m of $E_d(z,\lambda)$ (downwelling spectral radiance) profile and projecting a line to a depth of 0.0 m, and 0.96 is the transmittance across the air-sea interface, assuming a near zenith sun angle (Smith and Baker, 1986).

The equation for calculating $R_{rs}(l)$ from the above-water data is

$$R_{rs}(\lambda) = (S_{w+s} - S_{sky}\rho(\theta))/(\pi S_g/refl), \qquad (4)$$

where S_{w+s} is the measured signal from the water and includes both L_w and reflected skylight, S_{sky} is the measured signal from the sky, $\rho(\theta)$ is the Fresnel reflectance of the sea surface at measurement angle (θ) ($<3.5\%$ for the measurement angles), S_g is the measured signal from a gray Spectralon standard, and refl is the reflectivity of the gray standard. π converts the reflected radiance values to irradiance for this Lambertian diffuser.

Remote sensing pigment algorithms

An existing pigment algorithm developed for the CZCS satellite, which operated from 1978 to 1986 (Gordon et al., 1983), was tested in this study. The first step in the CZCS algorithm is the calculation of sensor-apparent total radiance, L_t, which is derived from the satellite digital counts with a calibration algorithm. Then L_w values are derived from the L_t values with an atmospheric correction algorithm. Finally the water leaving radiance values are used to derive the pigment concentrations (C) using one of two regression equations adopted by NASA (Gordon et al., 1983). The following equation is used first;

$$\log_{10}C = 0.053 + 1.71\log_{10}(L_w(550)/L_w(443)) \qquad (5)$$

At high pigment concentration $L_w(443)$ usually becomes too small to be retrieved from $L_t(443)$ with sufficient accuracy to be useful (Gordon et al., 1983). Therefore, if C derived from equation (5) is more than 1.5 mg /m^3, then C is determined from the following equation;

$$\log_{10}C = 0.522 + 2.44\log_{10}(L_w(550)/L_w(520)) \qquad (6)$$

The CZCS global algorithm is known to work well in Case 1 waters (Morel and Prieur, 1977) where the measured values, chlorophyll *a* plus phaeopigments, are usually covariant with CDOM and detritus, the other optically active components of the water. This covariance makes the algorithm successful, because the ratio of two spectral bands can account for only one variable. However, the global CZCS algorithm (Gordon *et al.*, 1983) was developed largely in subtropical waters and generally overestimates pigments in waters with high CDOM or suspended sediments (Hochman *et al.*, 1994) and often underestimates high-latitude pigments (Arrigo *et al.*, 1994). One reason for this variation is that the two components that affect water color the most, phytoplankton and CDOM, do not always covary. Thus the CZCS algorithm parameters are not universal.

The SeaWiFS algorithm tested in this paper was developed by Carder *et al.* (submitted). It uses a short wavelength channel (412 nm) to distinguish chlorophyll *a* from CDOM and degradation products, because both CDOM and particulate detritus absorb more strongly at 412 nm than at 443 nm, whereas the opposite is true for chlorophyll *a* (Carder *et al.*, 1991). The algorithm is based on a semi-analytical model of remote sensing reflectance (R_{rs}) and is an extension of the irradiance reflectance algorithm for chlorophyll *a* developed by Carder *et al.* (1991). Based on the shape of the absorption curve for phytoplankton versus those for CDOM and detritus, equations using spectral ratios of 412:443 and 443:555 for $R_{rs}(\lambda)$ provide a good separation of the two absorption contributions (Carder *et al.*, 1991). Since these equations are not easily solved algebraically, a lookup table (LUT) was created to store a(443)/a(412) and a(555)/a(443) total absorption ratios. Given an input spectrum of $R_{rs}(\lambda)$ values, the SeaWiFS algorithm first estimates the absorption coefficient of phytoplankton at 675 nm, $A_\phi(675)$, by means of the absorption due to phytoplankton at blue wavelengths. The absorption coefficient of CDOM at 400 nm, $A_g(400)$ is calculated at the same time. The LUT is then used to quickly search for absorption ratios that are just above and just below the modeled values. Modeled $A_\phi(675)$ and $A_g(400)$ values are then derived by interpolating between the LUT values. Finally, chlorophyll *a* is calculated from the modeled $A_\phi(675)$ values using a linear regression of log([chl *a*]) vs. log($A_\phi(675)$), which was evaluated using a number of subtropical, high-light, surface water sample data sets (Carder *et al.*, submitted).

Data input to pigment algorithms

The MER in-water data were input into both the SeaWiFS and CZCS chlorophyll *a* algorithms. The above-water data were input into the SeaWiFS algorithm, but were not input into the CZCS algorithm, because $E_d(0^-,\lambda)$ needed to calculate $L_w(\lambda)$ from R_{rs} (see equation (2)) could not be simultaneously measured using the single-sensor PS-II (a limitation which was later rectified by using a dual spectrometer system), or modeled reliably due to the partly cloudy conditions that prevailed during both time series. $L_w(\lambda)$ values, however, were derived from the in-water data and input into the CZCS algorithm. The in-water wavelengths matching most closely those required for the CZCS algorithm are 441 nm and 550 nm. No atmospheric corrections were needed since only in-water data extrapolated to the surface were used. Similarly, the SeaWiFS algorithm uses R_{rs} from the following six wavelengths in its computations; 412 nm, 443 nm, 490 nm, 510 nm, 555 nm and 670 nm. The hyperspectral above-water data contained these exact wavelengths, but the closest wavelengths available in the in-water L_u data (used to calculate R_{rs} using equations

(1) and (2) above) were 410 nm, 441 nm, 488 nm, 520 nm, 550 nm, and 683 nm. Since 683 nm is the fluorescence peak of chlorophyll *a* and was also a full 13 nm off of the required SeaWiFS wavelength of 670 nm, $L_u(671)$ was calculated from the in-water $E_u(671)$ channel using the equation;

$$L_u(z, \lambda) = E_u(z, \lambda)/Q(z, \lambda), \tag{7}$$

where $Q(z,\lambda)$ is the geometric factor relating L_u to E_u for each wavelength and at each depth. Q factors were calculated for 5 matching in-water L_u and E_u wavelengths (410, 441, 488, 520 and 550 nm), and a mean Q was then applied to the in-water $E_u(671)$ channel to calculate the required $L_u(671)$ for each cast. This mean Q factor ranged from 3.5 to 4.8 and falls within the experimental range found by Austin (1979), and Morel and Gentili (1993). Once again, no atmospheric corrections were needed since only surface and in-water data were used.

RESULTS

A linear regression plot of the CZCS pigment (using in-water data) vs. the measured surface chlorophyll *a* during both time series is shown in Fig. 2a. Figure 2b shows a linear regression plot of the SeaWiFS algorithm (using in-water data) vs. the measured surface chlorophyll a. Figure 2c shows a linear regression plot of the SeaWiFS algorithm (using above-water data) vs. the measured surface chlorophyll a. Figure 2d shows a linear regression plot of the SeaWiFS algorithm (using above-water data with 4 outlier points removed) vs. the measured surface chlorophyll a.

A linear regression between the CZCS algorithm using in-water data and measured surface chlorophyll gives a slope of 0.933 and a Y-intercept at 0.236, with an R^2 of 0.801 and a correlation coefficient of 0.895. A linear regression between the SeaWiFS algorithm using in-water data and measured surface chlorophyll gives a slope of 0.618 and a Y-intercept of 0.964, with an R^2 value of 0.543 and a correlation coefficient of 0.737 (see Table 1). A linear regression between the SeaWiFS algorithm using above-water data and measured surface chlorophyll gives a slope of 1.076 and a Y-intercept of 0.048, with an R^2 value of 0.671 and a correlation coefficient 0.819.

A null hypothesis that the difference between the chlorophyll values predicted by the CZCS algorithm using in-water data and the measured chlorophyll values are zero, could not be rejected using a two-tail sample t-test ($n = 32$; $\alpha = 0.05$). The results were the

Table 1.   *Statistics for combined Time Series I and II data.*

Algorithm Data Set	CZCS in-water	SeaWiFS in-water	SeaWiFS above-water	SeaWiFS above-water*
Data Points	32	32	27	23
Correlation	0.895	0.737	0.819	0.953
R squared	0.801	0.543	0.671	0.908
Sample t-test	Not Rejected	Not Rejected	Rejected	Not Rejected
Slope	0.933	0.618	1.076	0.937
Y-intercept	0.236	0.964	0.048	0.014

* Above-water data set with 4 outlier points removed and mean offset of 0.05 subtracted from data.
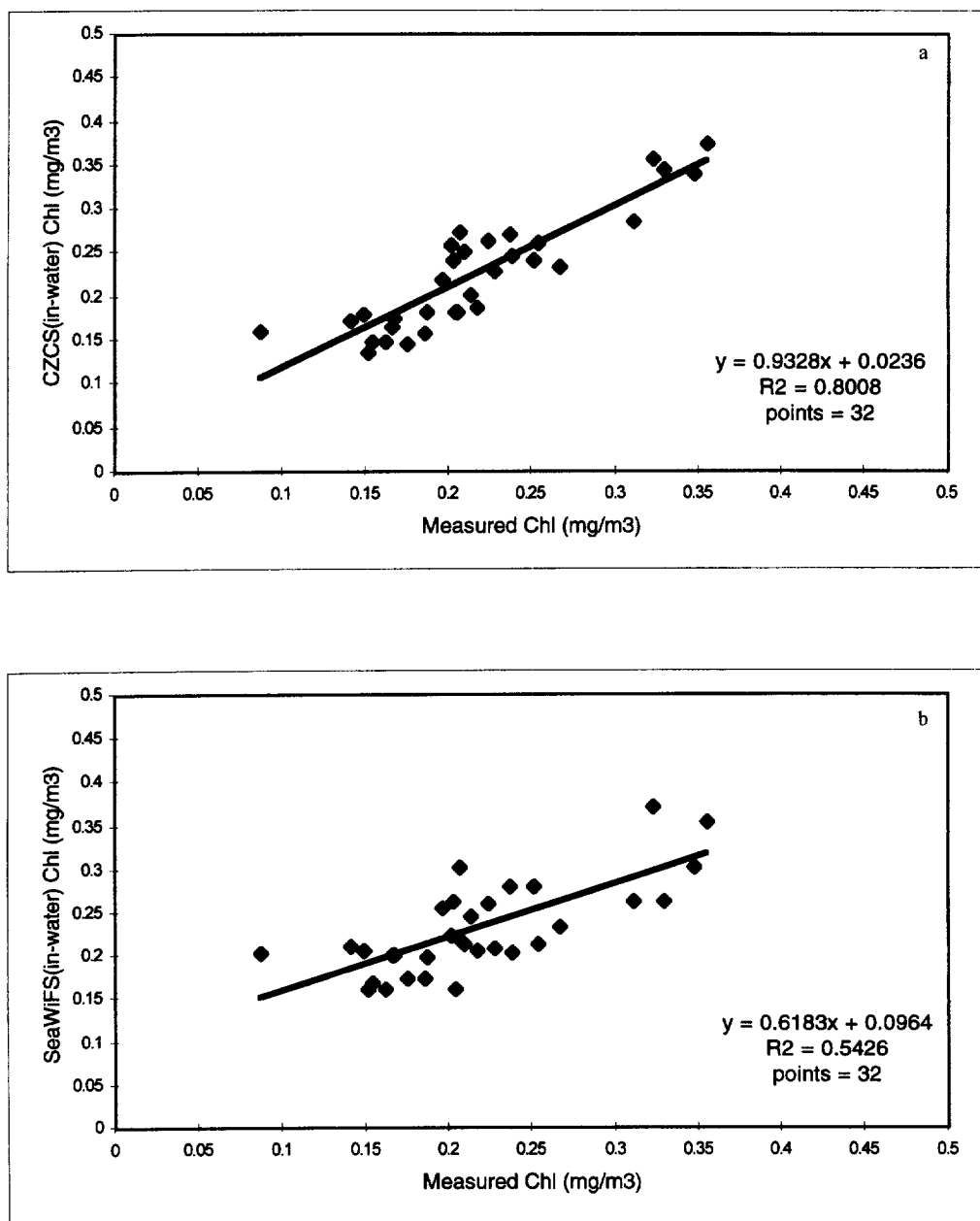
Fig. 2. a. Linear regression of CZCS algorithm using in-water data vs. measured surface Chlorophyll taken from the both Time Series. b. Linear regression of SeaWiFS algorithm using in-water data vs. measured surface Chlorophyll taken from both Time Series. c. Linear regression of SeaWiFS algorithm using above-water data vs. measured surface Chlorophyll taken from both Time Series. d. Linear regression of SeaWiFS algorithm using above-water data (with 4 outlier points (> 1 Std. Dev.) removed) vs. measured surface Chlorophyll taken from both Time Series.

y = 1.0756x + 0.0476
R2 = 0.6711
points = 27

y = 0.9365x + 0.063
R2 = 0.9078
points = 23
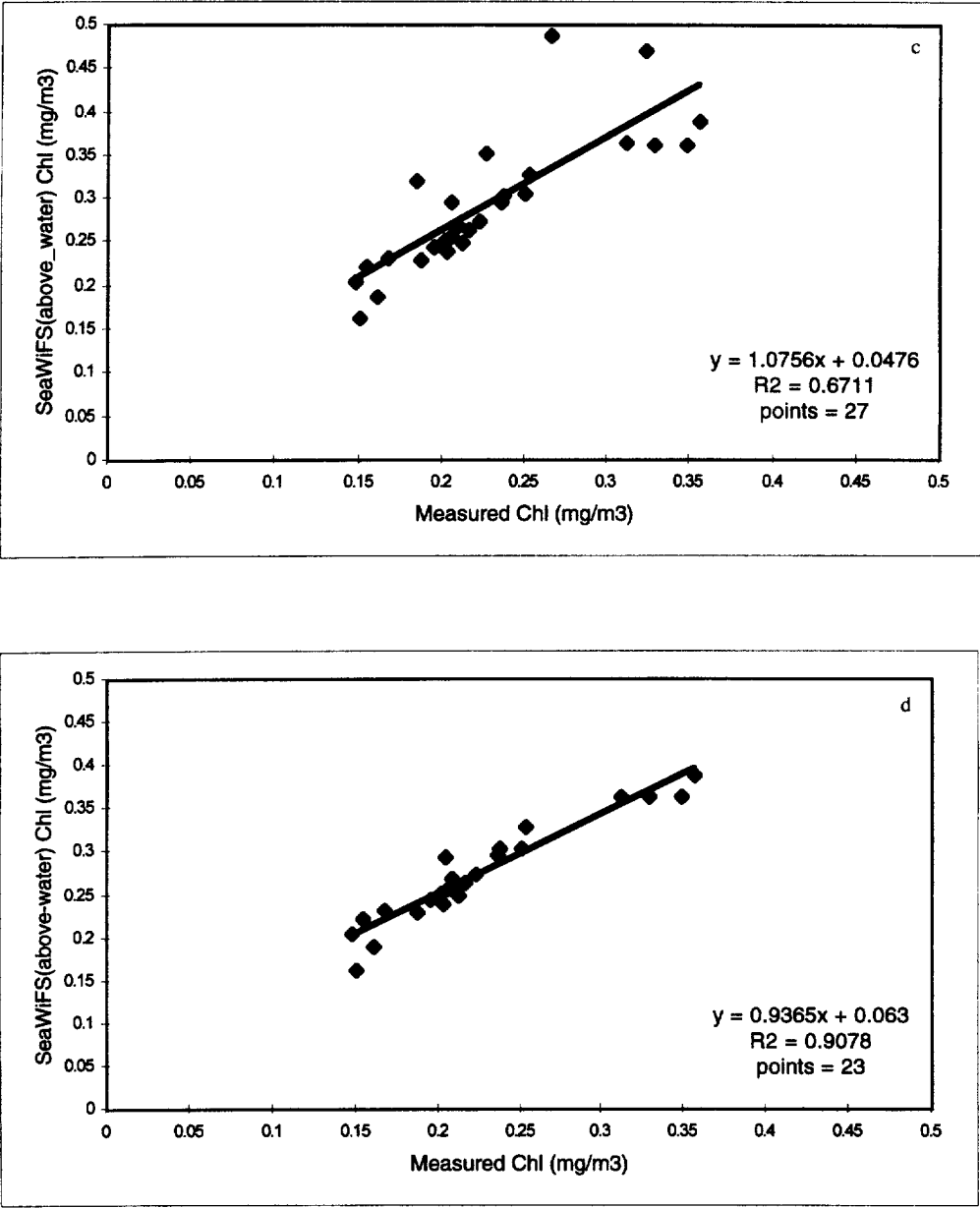
Fig. 2.   (c) and (d).

identical for the SeaWiFS algorithm using in-water data. However the null hypothesis was rejected for the SeaWiFS algorithm using above-water data ($n = 27$; $\alpha = 27$). This is due primarily to the overestimation (by a mean of 0.05 mg/m^3) of predicted chlorophyll by the SeaWiFS algorithm using the above-water data set. In addition, four points were greater than 1 standard deviation from the group mean. Removing these four points and

subtracting the mean 0.05 mg/m^3 allows the null hypothesis to not be rejected. In addition, the correlation coefficient increases to 0.953, and the R^2 value rises to 0.908, the highest values of the study.

DISCUSSION

Determination of direct biological response to physical events requires consideration of many factors that influence the ecosystem of the central equatorial Pacific Ocean which are difficult to match on a one-to-one basis. Physical forces such as wind-driven TIWs and remotely forced Kelvin waves control the supply of macro-nutrients (e.g., nitrate, phosphate and silicate) and micro-nutrients (e.g., iron) to the euphotic zone. The shear between the Southern Equatorial Current (SEC) and the Equatorial Undercurrent (EUC) drives the high rate of dissipation of turbulent kinetic energy at the equator and contributes greatly to mixing, and consequently to the distribution of nutrients (Carr *et al.*, 1995). Kelvin waves can reduce the upward flux of iron and macronutrients to surface waters by depressing the EUC below the depth of high vertical velocity, thus reducing phytoplankton growth rates. Remote detection of Kelvin waves using bio-optical data would be based on detecting a resulting decrease in chlorophyll *a* concentration. Conversely, a shallow more intense EUC created by a TIW would imply increased transport of iron and macronutrients to the surface, thereby enhancing near-surface phytoplankton growth rates, resulting in increases in remotely detectable surface chlorophyll concentrations.

Time Series I occurred during the maximum expression of the 1991–92 El Niño event, and also coincided with the peak of a passing Kelvin wave, which was identified from temperature and current data from the TOGA (Tropical Ocean Global Atmosphere) TAO (Tropical Atmosphere-Ocean) deep-ocean mooring array maintained by the National Oceanic and Atmospheric Administration (NOAA). Time Series II occurred during La Niña conditions and encompassed the complete passage of a TIW.

Derived chlorophyll *a* from the CZCS algorithm, using in-water data, tracked both qualitative and quantitative changes in measured surface chlorophyll *a* during both time series (Figs 3a and 3b). The SeaWiFS derived chlorophyll a, using the same in-water data, also tracked well with the measured surface chlorophyll *a* from both time series (Figs 4a and 4b).

A plot of SeaWiFS derived chlorophyll *a*, using the above-water reflectance data, with measured surface chlorophyll *a* for both time series is shown in Figs 5a and 5b. While the qualitative changes in chlorophyll *a* are tracked well by the algorithm, it overestimates all of the measured chlorophyll *a* values during both time series by a mean value 0.05 mg/m^3, as discussed previously. Also as discussed previously, two days during each time series had estimated chlorophyll *a* values that were greater than one standard deviation from the mean of each time series. A plot of SeaWiFS derived chlorophyll *a*, using the above-water data with these outlier points removed and with a mean offset of 0.05 subtracted, with measured surface chlorophyll *a* for both time series is shown in Fig. 6. The SeaWiFS derived chlorophyll *a* now tracks the measured chlorophyll *a* values very well.

SeaWiFS protocols (Mueller and Austin, 1995) call for using profiles of L$_u$ and E$_d$ to validate the estimates L$_w$ calculated from SeaWiFS data. Carder *et al.* (Submitted) used the above-water reflectance measurements to develop their SeaWiFS chlorophyll *a* algorithm. We get similar (but not identical) estimates of R$_{rs}$ from the above-water and in-water data (see Fig. 7). This was the first data set where we collected above-water
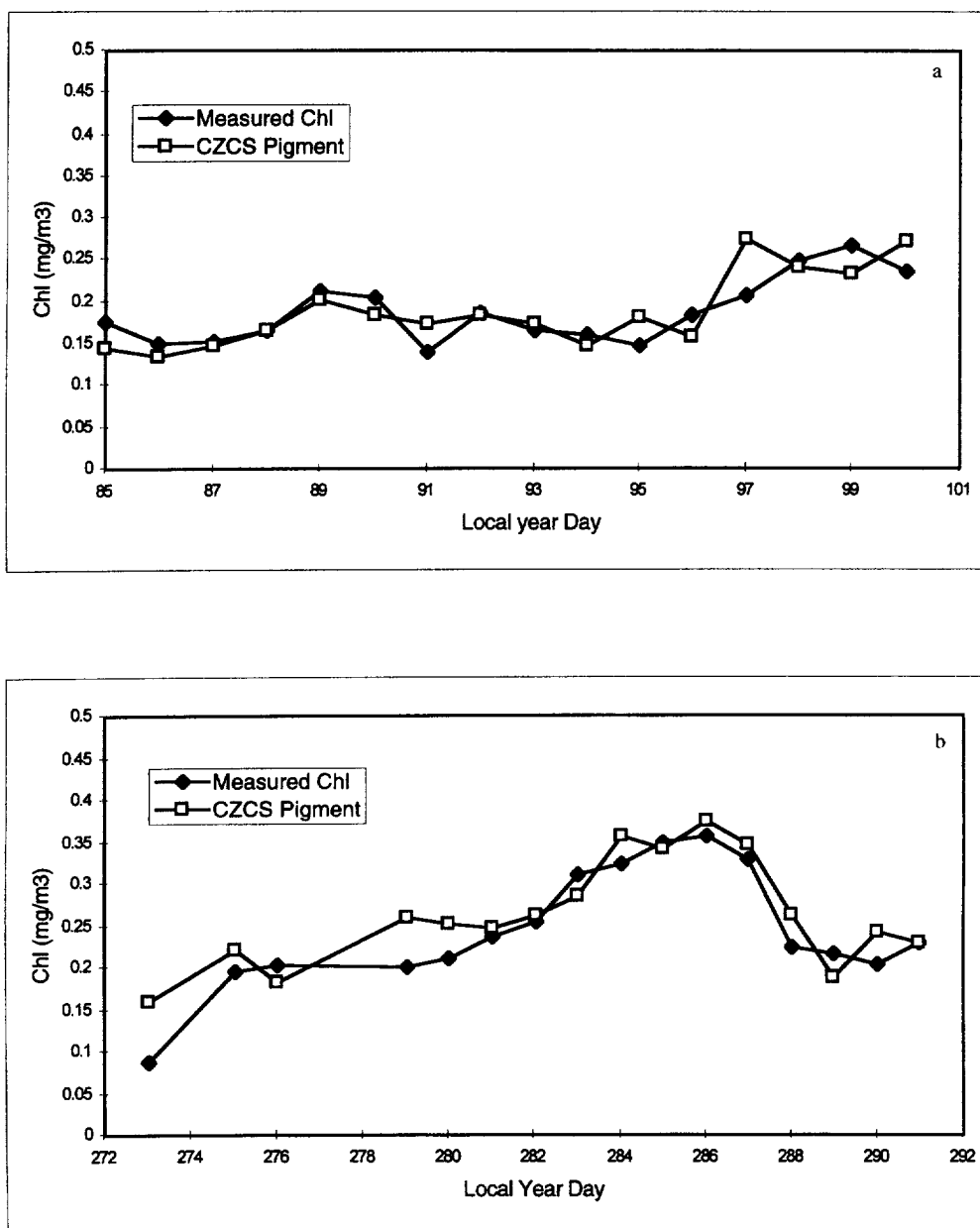
Fig. 3.   a. CZCS derived Chlorophyll (using in-water data) with measured surface Chlorophyll at
the Time Series I station. b. CZCS derived Chlorophyll (using in-water data) with measured surface
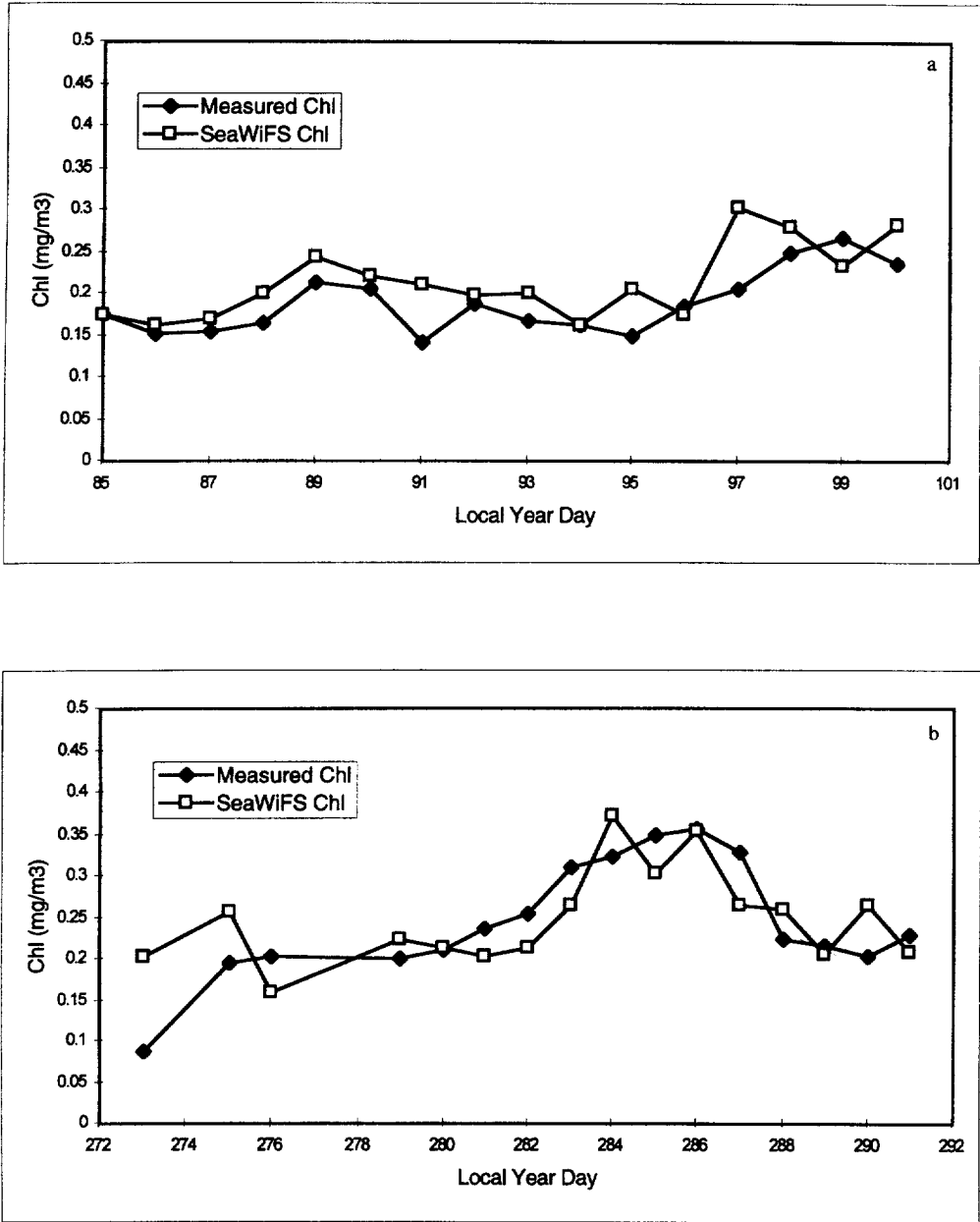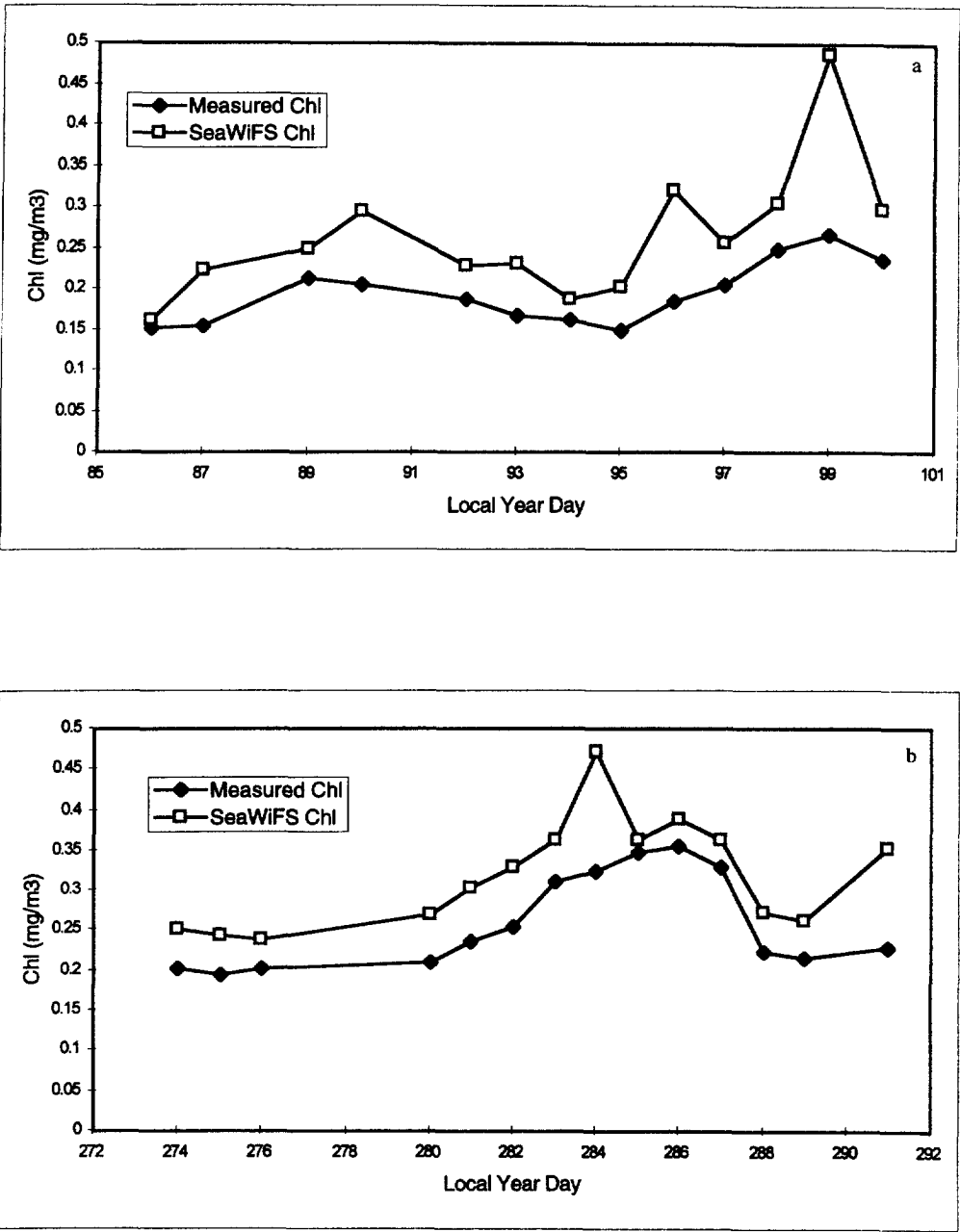Chlorophyll at the Time Series II station.

Fig. 4.   a. SeaWiFS derived Chlorophyll (using in-water data) with measured surface Chlorophyll at the Time Series I station. b. SeaWiFS derived Chlorophyll (using in-water data) with measured surface Chlorophyll at the Time Series II station.
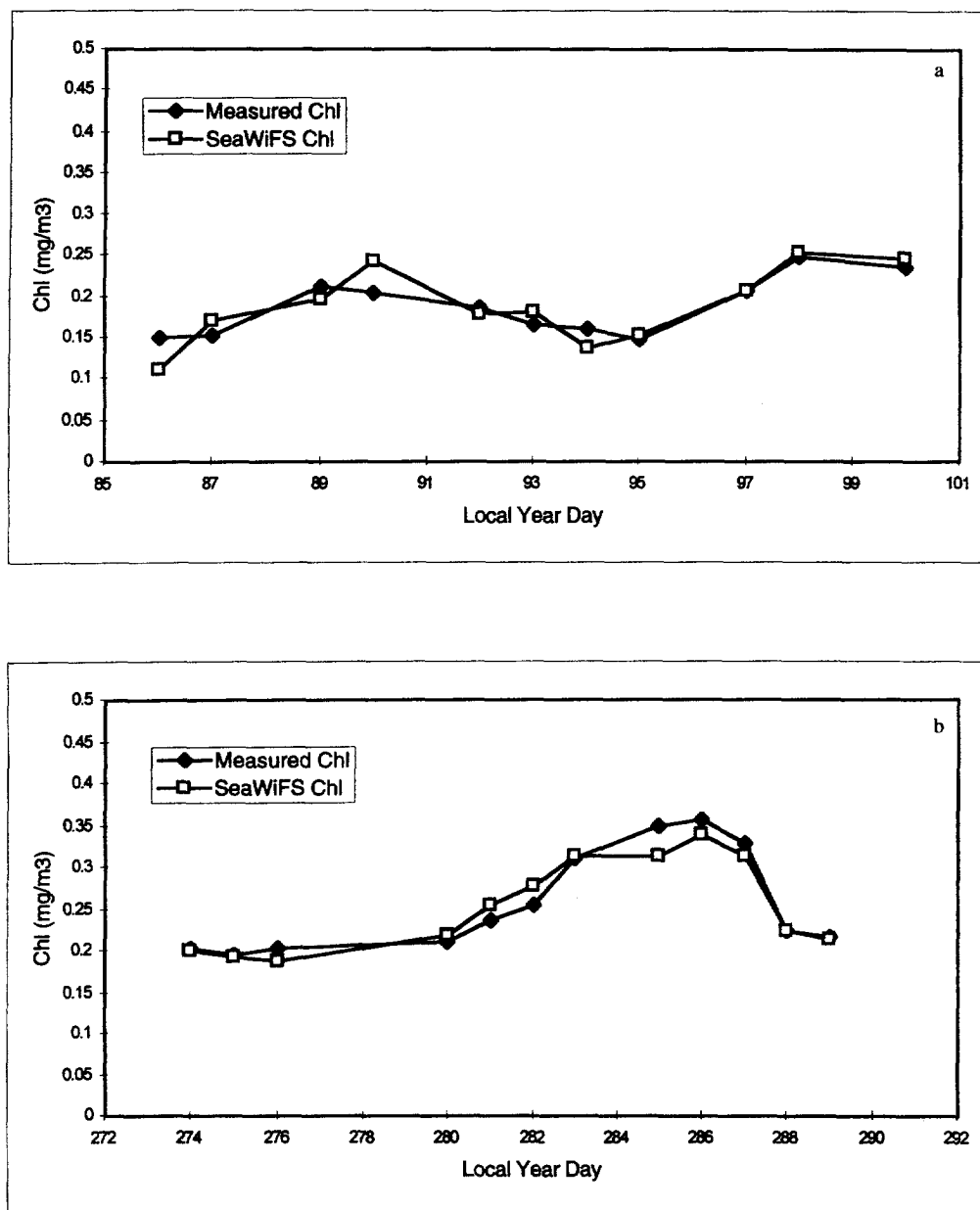
Fig. 5. a. SeaWiFS derived Chlorophyll (using above-water data) with measured surface Chlorophyll at the Time Series I station. b. SeaWiFS derived Chlorophyll (using above-water data) with measured surface Chlorophyll at the Time Series II station.

Fig. 6.   a. SeaWiFS derived Chlorophyll (using above-water data with two outlier points removed and with mean offset of 0.05 subtracted) with measured surface Chlorophyll at the Time Series I station. b. SeaWiFS derived Chlorophyll (using above-water data with two outlier points removed and with mean offset of 0.05 subtracted) with measured surface Chlorophyll at the Time Series II station.
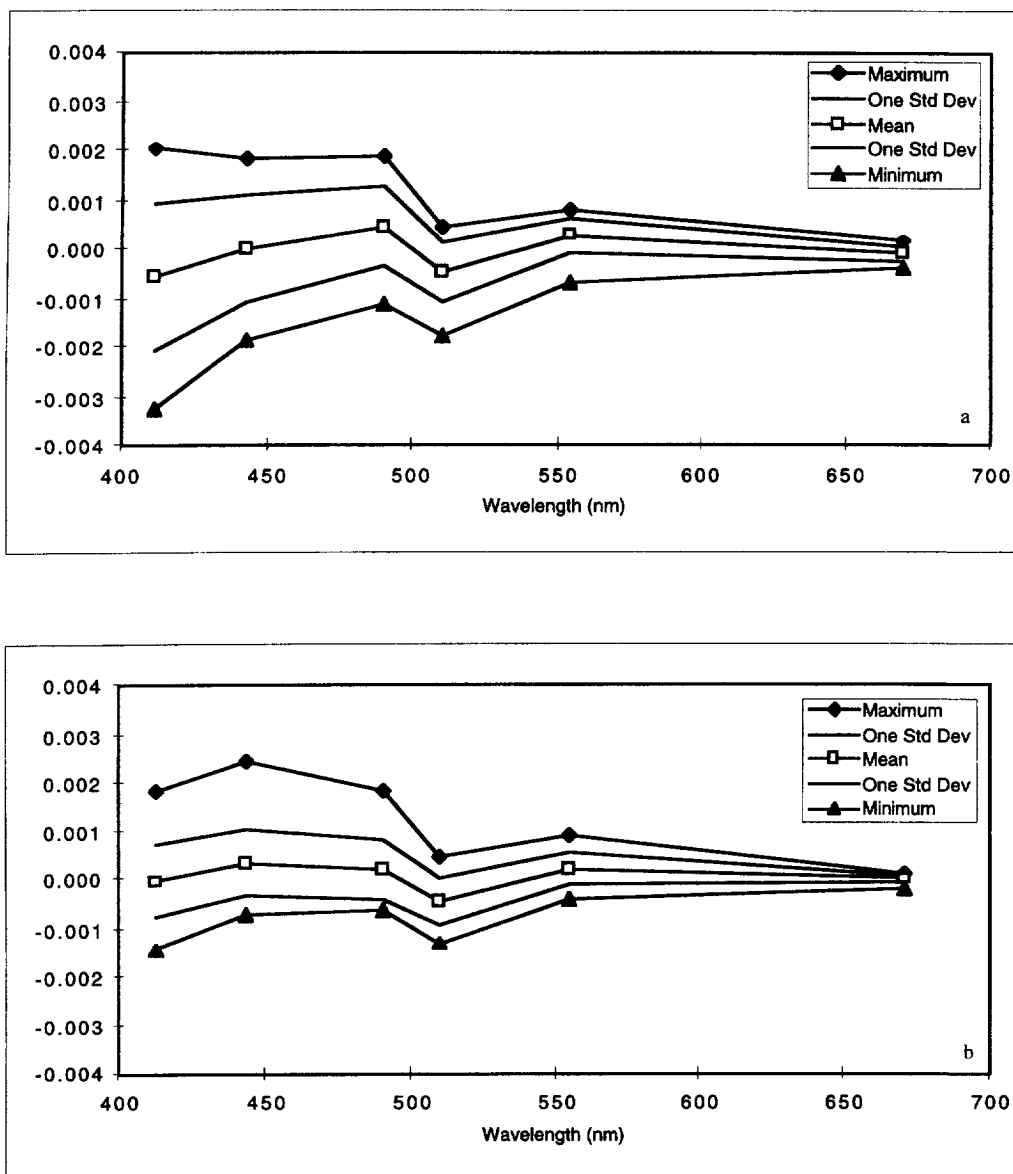
Fig. 7.   a. Comparison of R_{rs} (in-water) minus R_{rs} (above-water) for Time Series I. b. Comparison
of R_{rs} (in-water) minus R_{rs} (above-water) for Time Series II.

remote sensing reflectance data. It was a particularly difficult measurement to make because the sun was near zenith and there were variable cloudy conditions. For this particular data set we consider the in-water data the more reliable measurement. The greatest variation between the two measurements occurs in the shorter wavelengths where the SeaWiFS algorithm is the most sensitive. This could presumably cause the overestimation in predicted chlorophyll when using above-water data. We are working with Ken Carder, who developed the above-water method, and the SeaWiFS program to understand and resolve these differences.

SUMMARY

The results of this study indicate that the SeaWiFS algorithm is capable of determining both quantitative and qualitative changes in surface chlorophyll *a* from remotely sensed optical data in HNLC regions such as the Equatorial Pacific. At this time, the SeaWiFS optical data are validated by in-water optical profile data while the SeaWiFS chlorophyll *a* algorithm is validated with above water reflectance data. In this study, however, we have found that the SeaWiFS algorithm works as well, if not better, using the in-water profile data. Clearly validation experiments must include both types of data, and we must continue to work to resolve any remaining discrepancies in these two estimates of R_{rs}.

Using satellite ocean color data alone for the remote detection of Kelvin waves is difficult, because Kelvin waves have such long periods and can reduce phytoplankton standing stock and growth rates in near-surface water. However, Kelvin waves can be tracked by sea-surface height using satellite altimeter data and sea-surface temperature (SST) using Advanced Very High Reflectance Radiometer (AVHRR) data. When a Kelvin wave is detected by these other methods our results indicate that satellite ocean color data can be used to characterize the biological response to the Kelvin wave.

Conversely, because TIWs have a much shorter period and can enhance near-surface phytoplankton growth rates quickly, they are much easier to track using remotely sensed ocean color data. TIWs also have a strong SST signature (Legeckis, 1977) and the combined SST and ocean color data should enhance our understanding of the effect of TIWs on phytoplankton populations over the entire region they affect, or roughly from the equator to 5°N. These large areas can only be adequately sampled by remote sensing. Ideally this is combined with optical data from moorings to provide vertical profile and high frequency sampling.

REFERENCES

Arrigo, K. R., McClain, C. R., Firestone, J. K., Sullivan, C. W. and Comiso, J. C. (1994) A comparison of CZCS and in situ pigment concentrations in the Southern Ocean, *SeaWiFS Technical Report Series*, Vol. 13, S. B. Hooker and E. R. Firestone, Eds., 30–34.

Austin, R. W. (1974) Inherent spectral radiance signals of the ocean surface. *Ocean Color Analysis, SIO ref. 74-10,* 2.1-2.20.

Austin, R. W. (1979) Coastal zone color scanner radiometry. *Ocean Optics VI, SPIE,* **208,** 170–177.

Austin, R. W. (1980) Gulf of Mexico, ocean-colour surface-truth measurements. *Boundary-layer Meteorology,* **18,** 269–285.

Bidigare, R. R. and M. E. Ondrusek (submitted) Effects of the 1992 El Niño on distributions of phytoplankton pigments in equatorial Pacific waters. *Deep-Sea Research.*

Bidigare, personal communication, 1995.

Carder, K. L., Hawes, S. K., Baker, K. A., Smith, R. C., Steward, R. G. and Mitchell, B. G. (1991) Reflectance model for quantifying chlorophyll in the presence of productivity degradation products. *Journal of Geophysical Research,* **96,** 20599–20611.

Carder, K. L., S. K. Hawes and Z. Lee (submitted) SeaWiFS Algorithm for Chlorophyll and colored dissolved organic matter in a subtropical environment. *Journal of Geophysical Research.*

Carder, K. L. and Steward, R. G. (1985) A remote-sensing reflectance model of a red tide dinoflagellate off West Florida. *Limnology and Oceanography,* **30,** 286–298.

Carr, M. E., Lewis, M. R. and Kelly, D. (1995) A physical estimate of new production in the equatorial Pacific along 150W, *Limnology and Oceanography,* in press.

Chisholm, S. W. and Morel, F. M. M. (1991) What controls phytoplankton production in nutrient-rich areas of the open sea, *Limnology and Oceanography* (Special Issue), Vol. 36, No. 8.

Cullen, J. J. (1995) Status of the iron hypothesis after the Open-Ocean Enrichment Experiment. *Limnology and Oceanography,* **40,** 1336–1343.

Eriksen, C. C., Blumenthal, M. B., Hayes, S. P. and Ripa, P. (1983) Wind-generated equatorial Kelvin waves observed across the Pacific Ocean. *Journal of Physical Oceanography,* **13,** 1622–1640.

Gordon, H. R., Clark, D. K., Brown, J. W., Brown, O. P., Evans, R. H. and Broenkow, W. W. (1983) Phytoplankton pigment concentrations in the Middle Atlantic Bight: comparison of ship determinations and CZCS estimates. *Applied Optics,* **22,** 20–36.

Halpern, D., Knox, R. A. and Luther, D. S. (1988) Observations of 20-day period meridianal current oscillations in the upper ocean along the Pacific equator. *Journal of Physical Oceanography,* **18,** 1514–1534.

Hochman, H. T., Muller-Karger, F. E. and Walsh, J. J. (1994) Interpretation of the coastal zone color scanner signature of the Orinoco River Plume. *Journal of Geophysical Research* 99(C4), 7443–7455.

Hooker, S. B., et al. (1992) SeaWiFS Technical Report Series, Volume 1, An Overview of SeaWiFS and Ocean Color, *NASA Tech. Memo.* 104566, 1, 25 pp.

Johnson, E. S. and McPhaden, M. J. (1993) On the structure of intraseasonal Kelvin waves in the equatorial Pacific Ocean. *Journal of Physical Oceanography,* **23,** 1608–1625.

Kessler, W. S. and M. J. McPhaden (1995) Equatorial waves and the dynamics of the 1991-1993 El Niño. *Journal of Climatology,* in press.

Knox, R. A. and Halpern, D. (1982) Long range Kelvin wave propagation of transport variations in Pacific Ocean equatorial currents. *Journal of Marine Research,* **40,** 329–339.

Legeckis, R. (1977) Long waves in the eastern equatorial Pacific Ocean: A view from a geostationary satellite. *Science,* **197,** 1181–1197.

Lindley, S. T., Bidigare, R. R. and Barber, R. T. (1995) Phytoplankton photosynthesis parameters along 140°W in the equatorial Pacific. *Deep-Sea Research II,* **42,** 441–463.

Morel, A. and Gentili, B. (1993) Diffuse reflectance of oceanic waters II: Bi-directional aspects. *Applied Optics,* **32,** 6864–6879.

Morel, A. and Prieur, L. (1977) Analysis of variations in Ocean Color, *Limnology and Oceanography,* **22,** 709–722.

Mueller, J. L. and R. W. Austin (1995) Ocean Optics Protocols for SeaWiFS Validation, Revision 1, NASA Technical Memorandum 104566, Vol. 25, S. B. Hooker, E. R. Firestone and J. G. Acker, Eds., 66 pp.

Murray, J. W., Johnson, E. and Garside, C. (1995) A U. S. JGOFS Process Study in the equatorial Pacific (EqPac): Introduction. *Deep-Sea Research II,* **42,** 275–293.

Philander, S. G. H., Halpern, D., Hansen, D., Legeckis, R., Miller, L., Paul, C., Watts, R., Weisberg, R. and Wimbush, M. (1985) Long waves in the equatorial. *Pacific Ocean, EOS, Trans. Am. Geophys. Union,* **66,** 154.

Philander, S. G. H. (1990) El Niño, La Niña, and the Southern Oscillation. Academic Press, San Diego, 293 pp.

Smith, R. C., Booth, C. R. and Star, J. L. (1984) Oceanographic Bio-optical Profiling System. *Applied Optics,* **23,** 2791–2797.

Smith, R. C. and Baker, K. S. (1978) The bio-optical state of ocean waters and remote sensing. *Limnology and Oceanography,* **23,** 247–259.

Smith, R. C. and Baker, K. S. (1986) Analysis of ocean optical data II. *Ocean Optics VIII, SPIE*, **637**, 95–100.
Siegel, D. A., M. C. O'Brien, J. C. Sorensen, D. A. Konnoff, E. A. Brody, J. L. Mueller, C. O. Davis, W. J. Rhea and S. B. Hooker (1995) Results of the SeaWiFS Data Analysis Round-Robin, July 1994 (DARR-94), NASA Technical Memorandum 104566, Vol. 26, S. B. Hooker and E. R. Firestone, Eds., 49-52.